Journal of Metals, Materials and Minerals, Vol. 32, No. 2, pp. 11-23, 2022

Amino-containing polymer-coated magnetite nanoparticles as nano-adsorbents for bisphenol A: Synthesis, kinetic and thermodynamic study

Jakkrit TUMMACHOTE[1], Metha RUTNAKORNPITUK[1,2], Duangdao CHANNEI[1], Filip KIELAR[1,2], and Boonjira RUTNAKORNPITUK[1,2,*]

[1] *Department of Chemistry, Faculty of Science, Naresuan University, Phitsanulok 65000, Thailand*
[2] *Center of Excellence in Biomaterials, Faculty of Science, Naresuan University, Phitsanulok 65000 Thailand*

***Corresponding author e-mail:** boonjirab@nu.ac.th

Received date:
17 March 2022
Revised date
23 May 2022
Accepted date:
24 May 2022

Keywords:
Magnetite;
Nanoparticle;
Bisphenol A;
Nano-adsorbent;
Adsorption

Abstract

Magnetite nanoparticles coated with poly(dimethyl aminoethyl methacrylate) (PDMAEMA@MNPs) and their quarternized form (PQDMAEMA@MNPs) were successfully synthesized and used as nano-adsorbents for bisphenol A (BPA). The particles were spherical with the average particle size between 10 nm and 20 nm in diameter with a moderate degree of nanoclustering (*ca.*150 to 200 particles/cluster). In terms of adsorption properties, the PDMAEMA@MNPs exhibited a higher BPA adsorption capacity (1.05 mg·g^{-1} MNP at pH 9) than the quaternized form (0.50 mg·g^{-1} MNP at pH 9). Equilibrium isotherm, kinetic, and thermodynamic characteristics of BPA adsorption on the PDMAEMA@MNPs were investigated. It was found that the BPA adsorption on the MNPs reached an equilibrium within 5 min and the maximum adsorption capacity (q_e) was 9.88 mg·g^{-1}. The adsorption isotherm study results indicated that the BPA adsorption process on PDMAEMA@MNPs exhibited the best fit with the Freundlich model, and the adsorption kinetics followed the pseudo-second order model with the R^2 value of 1.00. The thermodynamic data exhibited a negative enthalpy change (ΔH° = -2585.571 J·mol^{-1}), indicating exothermic BPA adsorption, and a negative Gibbs free energy (ΔG°), implying a spontaneous BPA adsorption process.

1. Introduction

Bisphenol A (2,2-bis(4-hydroxyphenyl) propane; BPA) is an endocrine disruptive compound (EDC) that can mimic or block the biological activity of natural hormones, interfere with the transport and metabolic process of natural hormones, or block hormone receptors, causing risks to human health [1]. Low doses of BPA have been reported to cause endocrine dyscrasia, sexual dysfunction, cardiovascular diseases, diabetes, obesity, and carcinogenesis [2]. BPA is mainly used as a monomer in the production of polycarbonate plastics and epoxy resins [3,4]. Materials containing BPA were extensively used in many products such as thermal paper, food packaging, baby bottles, drink containers, medical devices, and internal coatings in tin cans [5-8]. Unfortunately, BPA can be gradually released from some of the products mentioned above, under normal conditions of use, into the surrounding environment. Even though its solubility in water is low (120 mg·L^{-1} to 300 mg·L^{-1}) [9], BPA has been detected in industrial wastewater, groundwater, surface water, and even drinking water [1,10]. In addition, it can enter the body through the ingestion system [11]. Hence, the removal and accurate monitoring of BPA present in water and wastewater are necessary for the sake of human health. Many techniques have been developed to remove BPA from water and wastewater including photocatalytic degradation, membrane separation, adsorption, and other processes [5,12-14]. Among these techniques, adsorption appears to be promising owing to its simple design and inexpensive and easy operation [7,15]. In recent years, many types of solid materials such as activated carbon [16], surface modified bio-adsorbents, polymeric adsorbents [1], zeolite [17], and Zinc oxide [18,19] have been developed for use as adsorbents to remove metals or organic compounds from waste streams.

Recently, magnetic nanoparticles, especially magnetite nano-particles (MNPs), have gained great amount of attention for potential uses in many applications, such as enzyme and protein immobilization [20], ribonucleic acid (RNA) and deoxyribonucleic acid (DNA) purification [21,22], and metal pre-concentration [23] and separation [24]. The suitability of MNPs for these task is attributed to their large surface area-to-volume ratio [25], good magnetic responsiveness [26], and ease in surface modification [27-29]. However, MNPs without surface stabilization tend to agglomerate when dispersed in liquid media due to inter-particle attractive forces, e.g., dipole-dipole interaction and magnetic force.

Coating the MNP surface with long chain polymers can prevent particle agglomeration due to steric stabilization [30]. In addition, it can also serve as a platform for binding with molecules or ions of interest [22,23,27,31-34]. Particularly in this work, coating MNP surface with poly(dimethyl aminoethyl methacrylate) (PDMAEMA)

is of great interest because the tertiary amino groups in this polymer can be protonated/deprotonated and easily quaternized to obtain a permanently positively charged polymer [35,36]. PDMAEMA-coated MNPs have been reported for use in protein [37] and DNA adsorption [38]. However, the study of the use of PDMAEMA-coated MNPs as nano-adsorbents for BPA is rather limited [2].

Thus, the novelty of this work was the demonstration of the facile synthesis and surface modification of MNPs with PDMAEMA (PDMAEMA@MNPs) and quarternized PDMAEMA (PQDMAEMA @MNPs) to be used as nano-adsorbents for BPA in aqueous media. BPA is an organic compound with hydrophobic aromatic groups and hydrophilic hydroxyl groups. This amphiphilic nature makes BPA molecule a good model compound for this work [8]. The synthesized MNPs exhibited good water dispersibility due to their high hydrophilicity and were easily separated from the dispersion by a magnet. These two types of the nano-adsorbents were well characterized via various techniques such as fourier transform infrared spectrophotometry (FTIR), thermogravimetric analysis (TGA), transmission electron microscopy (TEM), scanning electron microscopy (SEM), Brunauer-Emmett-Teller (BET) technique, and photo correlation spectroscopy (PCS). Adsorption efficiency of the nano-adsorbents and the optimization of the adsorption parameters (e.g. solution pH, amounts of the nano-adsorbents, and BPA concentrations) were investigated. In addition, the BPA adsorption isotherm, kinetics, and thermodynamics were studied as well.

2. Experimental

2.1 Materials

The following reagents were used as received; iron(II) chloride tetrahydrate ($FeCl_2{\cdot}4H_2O$) (99%, Acros Organics), iron(III) chloride anhydrous ($FeCl_3$) (98%, Acros Organics), ammonium hydroxide 30% (NH_4OH) (Carlo Erba), oleic acid (Carlo Erba), 3-(trimethoxysily) propyl methacrylate (TMSPMA) (98%, Aldrich), 2-(dimethylamino) ethyl methacrylate (DMAEMA) (99%, Acros Organics), 2,2′-azobis (2-methylpropionitrile) (AIBN) (98%, Sigma-Aldrich), iodomethane stabilized with silver (CH_3I) (99%, Merck), n-hexane (Carlo Erba), triethylamine (TEA) (99%, Merck), tetrahydrofuran (THF) (99.8%, RCI Labscan), acetonitrile (ACN) (99.9%, RCI Labscan), toluene (99.5%, RCI Labscan) and acetone (99.5%, RCI labscan). 1,4-Dioxane (99.8%, RCI Labscan) was dehydrated using molecular sieves before use.

2.2 Instrument

UV/Visible absorption measurements were obtained *via* high performance liquid chromatography (HPLC) (HPLC 1100series, Agilent). TEM analysis was acquired *via* Tecnai 12, Philips TEM, operated at 120 kV and equipped with a Gatan model 782 CCD camera. The particles were redispersed in water and sonicated before deposition on a TEM grid. FTIR was carried out on Spectrum GX, Perkin Elmer FTIR instrument in the ATR mode. Hydrodynamic size and zetapotential values were measured using PCS (Nano ZS4700, Malvern). Magnetic properties were analyzed by VSM using magnetic moment in the range of ±10,000 G (Standard 7403 Series, Lakeshore). TGA was performed at temperatures ranging from 25°C to 600°C with the heating rate of 20°C·min^{-1} under oxygen atmosphere (Thermo Plus TG8120, Rigaku). The morphologies of the nano-adsorbents were carried out *via* field emission scanning electron microscopy (FESEM) (AperoS, Thermo Fisher Scientific) with 20 kV accelerating voltage and the analysis of the elements (Fe, C, N, O) was performed *via* energy-dispersive X-ray (EDX) (Oxford Instruments, Oxford). The surface area was analyzed *via* Brunauer-Emmett-Teller (BET) technique (Nova2200e, Quantachrome). X-ray diffraction (XRD) of the nano-adsorbents were carried out using a Bruker D2 PHASER X-ray diffractometer.

2.3 Synthesis of PDMAEMA@MNPs and PQDMAEMA @MNPs

2.3.1 Synthesis of methacrylate-coated magnetite nanoparticles (MA-coated MNPs)

Bare MNPs were prepared *via* a co-precipitation method as follows. $FeCl_2{\cdot}4H_2O$ (1 g, 5×10^{-3} mol) and $FeCl_3$ (1.66 g, 1×10^{-2} mol) were dissolved in distilled water (40 mL), followed by the addition of ammonium hydroxide solution (30%, 20 mL). After 30 min of stirring, the formed MNPs were magnetically separated from the mixture and repeatedly washed with distilled water. The MNPs were then redispersed in an oleic acid solution (2 mL of oleic acid in 20 mL of toluene) and stirred for 30 min. The oleic acid-coated MNPs were separated by a magnet, repeatedly washed with acetone, and dried *in vacuo*. To prepare MA-coated MNPs, the oleic acid-coated MNPs (0.5 g) were redispersed in toluene (20 mL), followed by the addition of TMSPMA (5.15 mL, 2.12×10^{-2} mol) and TEA (1 mL, 7.17×10^{-3} mol) and stirred for 24 h under N_2 atmosphere at room temperature. The modified MNPs were magnetically separated, repetitively washed with hexane, and dried *in vacuo* to obtain the MA-coated MNPs in a 90.5 % yield.

2.3.2 Synthesis of poly(dimethylaminoethyl methacrylate)-coated magnetite nanoparticles (PDMAEMA@MNPs)

MA-coated MNPs (0.1 g) were redispersed in 1,4-dioxane (26 mL) under N_2 atmosphere followed by the addition of DMAEMA (5.24 mL, 3×10^{-2} mol) and AIBN (0.05 g, 3×10^{-4} mol). The reaction was stirred at 70°C for 30 min. After the reaction, the particles were magnetically separated, repeatedly washed with 1,4-dioxane, distilled water, and dried *in vacuo* to obtain the PDMAEMA-coated MNPs in a 68.4%yield.

2.3.3 Synthesis of quarternize poly(dimethylaminoethyl methacrylate)-coated magnetite nanoparticles (PQDMAEMA @MNPs)

A dispersion of PDMAEMA@MNPs (100 mg in 5 mL of THF) was mixed with CH_3I (5 mL, 8×10^{-2} mol). The quarternization reaction was performed in an ultrasonic bath for 3 h in the dark. The MNPs were magnetically separated, repeatedly washed with THF, distilled water, and dispersed in distilled water (40 mL) to obtain the PQDMAEMA-coated MNPs solution in an 84%yield (0.0021 g of the particle/mL).

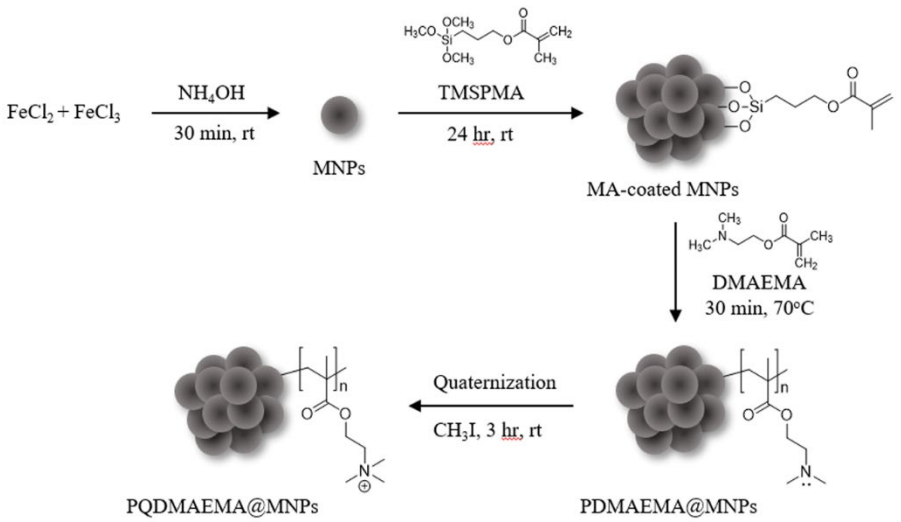

Scheme 1. Synthesis of PDMAEMA@MNP and PQDMAEMA@MNP nano-adsorbents.

2.4 Quantitative analysis of BPA

BPA was quantitatively analyzed *via* HPLC equipped with a C18 column (25 mm × 5 mm) with a diode array detector at 229-nm wavelength and with an acetonitrile (ACN):H_2O mixture (1:1 ratio) used as the mobile phase with 1 mL·min^{-1} flow rate. All sample solutions were filtered through 0.45-µm filters before each measurement. The reported values are the average of at least five measurements.

2.5 Determination of BPA adsorption efficiency of PDMAEMA@MNPs and PQDMAEMA@MNPs

BPA adsorption efficiency on the nano-adsorbents was investigated using an HPLC technique (Scheme 2). The effect of solution pH on BPA adsorption efficiency was studied first. One mg of the nano-adsorbents was dispersed in phosphate buffer solutions having different pH values (10 mM, pH 6 - pH 10) and then 500 µL of BPA solution (5 ppm in water**)** was added into the nano-adsorbent dispersion. The mixture was shaken for 5 min at room temperature and the particles were magnetically separated. The BPA adsorbed on the nano-adsorbents was desorbed by washing with methanol (200 µL) and sonication for 3 min. After magnetic separation to remove the MNPs, the desorbed BPA solutions were filtered through 0.45-µm filters for quantitative analysis *via* HPLC. All reported results are the average of at least three repeated tests.

2.6 Study in adsorption parameters

BPA adsorption capacity (q_e, mg/g) of the nano-adsorbents was estimated using Equation 1 [12].

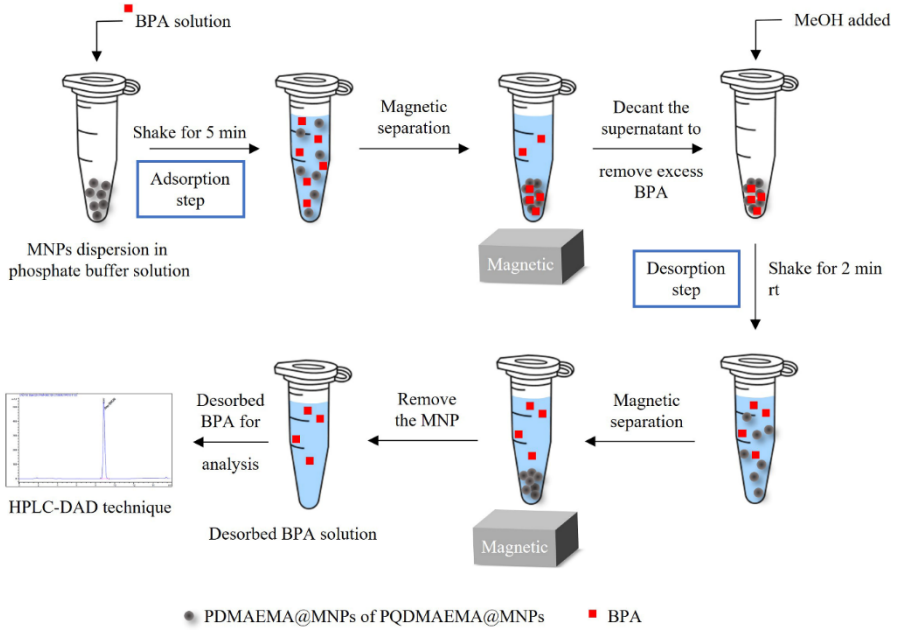

Scheme 2. Adsorption-desorption process of BPA on the nano-adsorbents.

$$q_e = \frac{(C_0 - C_e)}{m} V \quad (1)$$

where C_0 and C_e (mg·L^{-1}) are the initial and equilibrium concentrations of BPA in solution, V (L) is the volume of the solution, and m (g) is the mass of the nano-adsorbents.

The Langmuir equation in the linear form used to predict the monolayer coverage of BPA on the surface of the nano-adsorbents is shown in Equation 2 [12].

$$\frac{C_e}{q_e} = \frac{C_e}{q_m} + \frac{1}{q_m K_L} \quad (2)$$

where C_e is the equilibrium concentration of BPA in solution (mg·L^{-1}), q_m is the maximum adsorption capacity of the nano-adsorbents (mg/g), and K_L (L·mg^{-1}) is the Langmuir constant related to the affinity of the binding sites. The parameters were calculated from the slope and the intercept of the plot of C_e/q_e versus C_e.

The Freundlich equation in the nonlinear form used to predict the multilayer coverage of BPA on the surface of the nano-adsorbents is shown in Equation 3 [12].

$$\ln q_e = \left(\frac{1}{n}\right) \ln C_e + \ln K_f \quad (3)$$

where K_f (mg·g^{-1}) is the Freundlich constant indicating the adsorption capacity and n is the adsorption strength. These constants were calculated from the slope and the intercept of the plot of $\ln q_e$ versus $\ln C_e$

Kinetic analysis of the adsorption process was carried out using the pseudo-first-order and pseudo-second-order models. The pseudo-first-order and the pseudo-second-order kinetic models were calculated from the experimental data at different adsorption times. The pseudo-first-order model can be expressed as shown in Equation 4 [39].

$$\log(q_e - q_t) = \log q_e - \left(\frac{k_1}{2.303}\right) t \quad (4)$$

where q_e (mg·g^{-1}) is adsorption capacity at equilibrium, q_t (mg·g^{-1}) is the adsorption capacity at time t (min), and k_1 (min^{-1}) is the equilibrium rate constant of the pseudo-first order process. The values of k_1 and q_e were calculated from the slope and the intercept of the plot of $\log(q_e - q_t)$ versus t, respectively.

The pseudo-second-order model is utilized under the assumption that the adsorption follows the second-order mechanism. The rate of occupation of adsorption sites is proportional to the square of the number of unoccupied sites. The pseudo-second-order model can be expressed as shown in Equation 5 [39].

$$\frac{t}{q_t} = \frac{1}{k_2 q_e^2} + \frac{1}{q_e} t \quad (5)$$

where k_2 is the pseudo-second order rate constant (g·mg^{-1}·min^{-1}). The value of q_e was calculated from the slope of the plot of t/q_t versus t.

The thermodynamic parameters were investigated by varying the dispersion temperatures from 30°C to 70°C. K_c is the equilibrium constant, and it was calculated from Equation 6,[11] where C_0 and C_e (mg·L^{-1}) are the initial and equilibrium concentrations of BPA in the solution. The enthalpy change (ΔH°) and the entropy change (ΔS°) were calculated from the straight line of the plot of $\ln K_c$ and $1/T$ according to Equation 7 [39].

$$K_c = \frac{C_e}{C_0 - C_e} \quad (6)$$

$$\ln K_c = \frac{\Delta S^\circ}{R} - \frac{\Delta H^\circ}{RT} \quad (7)$$

These values can be used to calculate ΔG° from the Gibbs relation as shown in Equation 8 [39].

$$\Delta G^\circ = \Delta H^\circ - T\Delta S^\circ \quad (8)$$

where ΔG° is calculated from the equation at temperatures from 303 to 343 K.

3. Results and discussion

3.1 Characterization of the MNPs

FTIR spectra of the MNPs from each step are shown in Figure 1. The spectrum of bare MNPs shows the Fe-O stretching vibrations of the MNP core at 549 cm^{-1} (Figure 1(a)). After the MNP coating with TMSPMA, the spectrum exhibits many characteristic signals of TMSPMA including peaks at 971 cm^{-1} (Si-O stretching), 1164 cm^{-1} (C-O stretching), 1631 cm^{-1} (C=C stretching), 1696 cm^{-1} (C=O stretching), and 2924 cm^{-1} (C-H stretching) indicating the presence of methacrylate (MA) on the MNP surface (Figure 1(b)) [40]. After the polymerization reaction, the spectrum of polymer-coated MNPs shows the characteristic signals of PDMAEMA (Figure 1(c)) (C-N stretching vibration at 1260 cm^{-1} and a sharp peak of C=O stretching at 1716 cm^{-1}). After the quaternization reaction, the spectrum of the MNPs exhibits similar characteristic signals as those of PDMAEMA @MNPs as shown in Figure 1(d) (C-N stretching at 1227 cm^{-1} and a sharp signal of C=O stretching at 1715 cm^{-1}) [41,42]. These results confirm the presence of the polymers coated on the MNP surface.

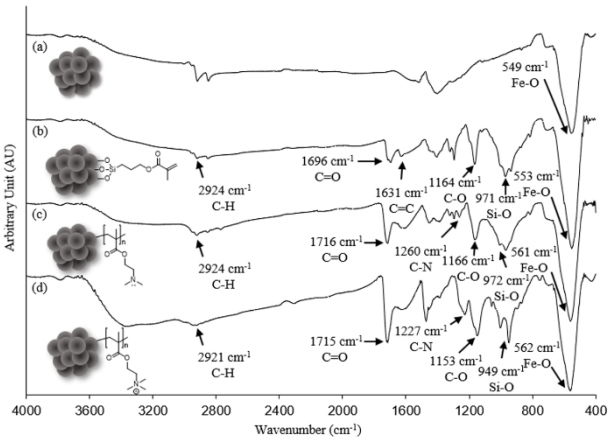

Figure 1. FTIR spectra of (a) bare MNPs, (b) MA-coated MNPs, (c) PDMAEMA @MNPs, and (d) PQDMAEMA@MNPs

The TGA technique was used to determine the percentage of organic components grafted on the MNPs (Figure 2(a)). The residue weight at the end of the experiment was assumed to be the weight of iron oxide from the MNP core, while the weight loss was attributed to the organic components in the nano-adsorbent. The TGA results for the bare MNPs show a weight loss of 15 wt%, which was attributed to the removal moisture absorbed on the particles [23]. Additional weight losses of *ca.*21 wt% and *ca.*25 wt% observed for PDMAEMA @MNPs and PQDMAEMA@MNPs, respectively, were attributed to the polymers grafted on the MNPs. The percent weight loss of the quarternized particles was slightly higher than that of the precursor ones due to the additional methyl groups in the polymer chains.

Magnetic properties of bare MNPs, PDMAEMA@MNPs, and PQDMAEMA@MNPs were investigated *via* the VSM technique (Figure 2b). Figure 2b indicates that the bare MNPs had a saturation magnetization value (M_s) of 69 emu·g^{-1} while the value for PDMAEMA @MNPs was 61 emu·g^{-1}. The slight decrease in the M_s was attributed to the existence of non-magnetic polymer layers on the particles. The M_s value of the PQDMAEMA@MNPs was further decreased (59 emu·g^{-1}) owing to the additional methyl groups in their structure.

The particle sizes of the two nano-adsorbents and their distributions were investigated using the TEM technique. PDMAEMA@MNPs were spherical with 10 nm to 20 nm in diameter and exhibited a moderate degree of nanoclustering (*ca.*150 to 200 particles/cluster) (Figure 3(a)). After the quarternization, PQDMAEMA@MNPs showed some improvement in water dispersibility with a lower degree of nanoclustering (Figure 3(b)). The presence of the polymer layers was also observed on the surface of the particles as indicated by the arrows in Figure 3 and in the supporting information (Figure S1). This was attributed to the increase in electrostatic repulsion of the positively charged quarternized polymers present on the MNP surface.

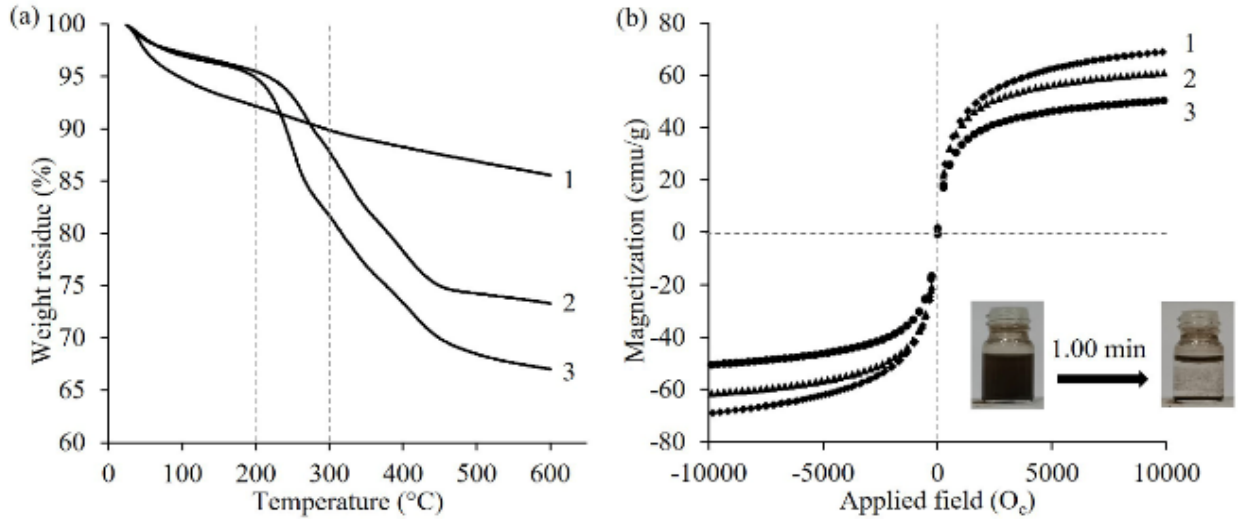

Figure 2. (a) TGA and (b) VSM curves of (1) bare MNPs, (2) PDMAEMA @MNPs, and (3) PQDMAEMA@MNPs.

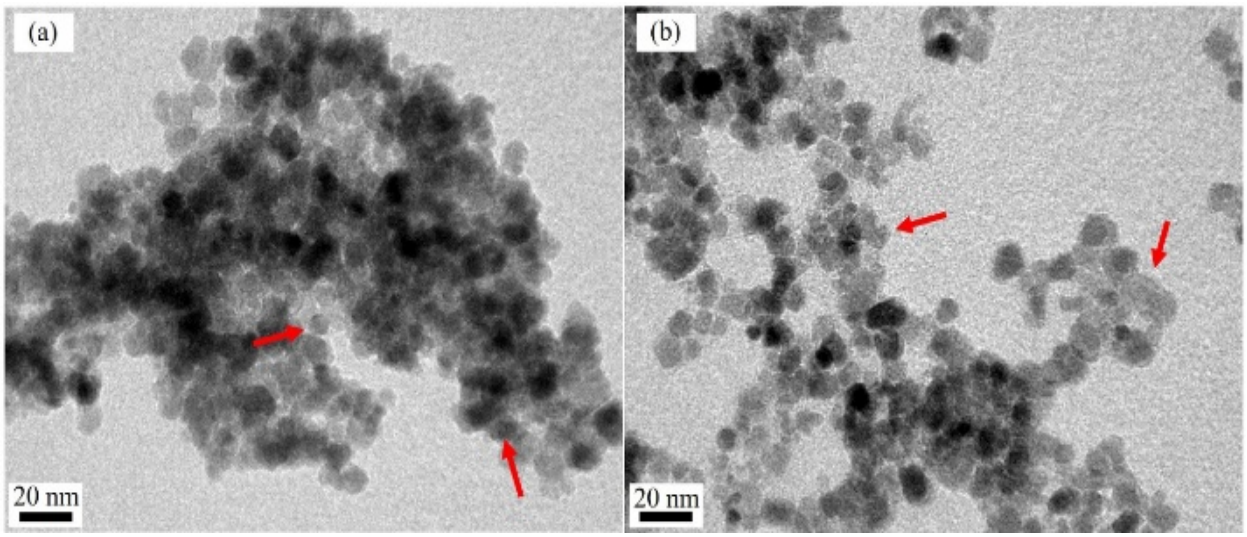

Figure 3. TEM images of (a) PDMAEMA@MNPs and (b) PQDMAEMA @MNPs nano-adsorbents.

Since the polymers used in this work possess a pH-responsive moiety [41-43], the effect of pH change on surface charge of the particles was investigated *via* PCS (Figure 4(a)). The results of the PCS experiment indicate that the surface charge (zeta potential value) of the PDMAEMA@MNPs is positive when dispersed in buffer solutions with pH 7 to pH 8 due to the protonation of the amino groups in the DMAEMA units, while the charge of the particles drastically decreased in buffer solutions with pH values from 9 to 11 due to their deprotonation. In contrast, PQDMAEMA@MNPs showed only a slight decrease in surface charge with increasing solution pH and this was attributed to the presence of the quarternary ammonium groups in their structure. The hydrodynamic sizes (D_h) of the PDMAEMA @MNPs and the PQDMAEMA@MNPs were also investigated in solutions with various pH values (Figure 4(b)). Their D_h values were responsive to the change in the pH of the dispersion media. In contrast to the PDMAEMA@MNPs, the D_h of the PQDMAEMA@MNPs increased stepwise when the solution pH increased from 7 to 9 and remain stable for pH values from 9 to 11. It should be noted that D_h of the PQDMAEMA@MNPs was higher than that of the PDMAEMA @MNPs at all pH values. This was attributed to the existence of positive charge of PQDMAEMA coated on the MNPs, allowing for more repulsive interactions between the quarternized chains and more water molecules being adsorbed in their structure.

Surface area, pore volume and pore size of the MNPs can significantly influence the adsorption properties. BET surface areas and Barrette Joynere Halenda (BJH) pore size and pore volume of the MNPs were thus investigated using N_2 adsorption/desorption measurements at 77 K. All samples exhibited typical type IV of isotherms with an H4 hysteresis loop, associated with the presence of mesoporous (20 Å to 500 Å) slit-shaped pores [44]**.** The surface properties obtained from the N_2 adsorption/desorption isotherms of these two kinds of adsorbents are summarized in Table 1. The surface area of PDMAEMA@MNPs (126.639 $m^2 \cdot g^{-1}$) was higher than that of PQDMAEMA@MNPs (94.396 $m^2 \cdot g^{-1}$). The increase of surface area agreed well with the increase of pore volume from *ca.*0.233 to 0.557 $cm^3 \cdot g^{-1}$ (PQDMAEMA@MNPs *vs* PDMAEMA @MNPs), relating to the N_2 gas adsorption-desorption capacity shown in the supporting information (Figure S2). This indicated that the surface properties played a significant role in the uptake of BPA on the surface of the adsorbents. PDMAEMA@MNPs exhibited a higher surface area and pore volumes than PQDMAEMA@MNPs, meaning that they have a higher feasibility for beneficial BPA adsorption.

3.2 Effect of the solution pH on BPA adsorption capacity

BPA adsorption capacity of the MNPs in the pH range from 6 to 10 was investigated (Figure 5). The experiment was carried out using 1 mg of the MNPs dispersed in 5 ppm-BPA solution. BPA adsorption capacity (qe) was calculated from the BPA calibration curve and an example of the calculation of BPA adsorption capacity (qe) is shown in the supporting information. These results indicated that PDMAEMA@MNPs had a higher adsorption capacity than those of PQDMAEMA@MNPs in every pH and they were in good agreements with those obtained from BET, indicating their high surface area, pore volume and average pore size as compared to those of the quaternized MNPs. In addition, the different degrees in their surface charge might play an important role in BPA adsorption capacity. The presence of the positively charged quaternary ammonium groups might somewhat inhibit the interaction between BPA and the polymers coated on the MNP surface. BPA adsorption capacity of PDMAEMA@MNPs increased stepwise from pH 6 to pH 9 and slightly dropped at pH 10, while that of the quarternized particles slowly increased from pH 6 and remained constant at pH 9 and 10. This suggests that the deprotonated form of BPA at pH values above its pK_a might somewhat influence the BPA adsorption capacity on PDMAEMA@MNPs (pK_a value of BPA is 9.60) [45]. Owing to their better adsorption capacity, the PDMAEMA@MNPs were thus used in further experiments.

Table 1. BET analysis of PDMAEMA@MNPs and PQDMAEMA@MNPs.

Sample	Surface area ($m^2 \cdot g^{-1}$)	Pore volume ($cm^3 \cdot g^{-1}$)	Average pore size (Å)
PDMAEMA@MNPs	126.639	0.557	104.053
PQDMAEMA@MNPs	94.396	0.233	69.106

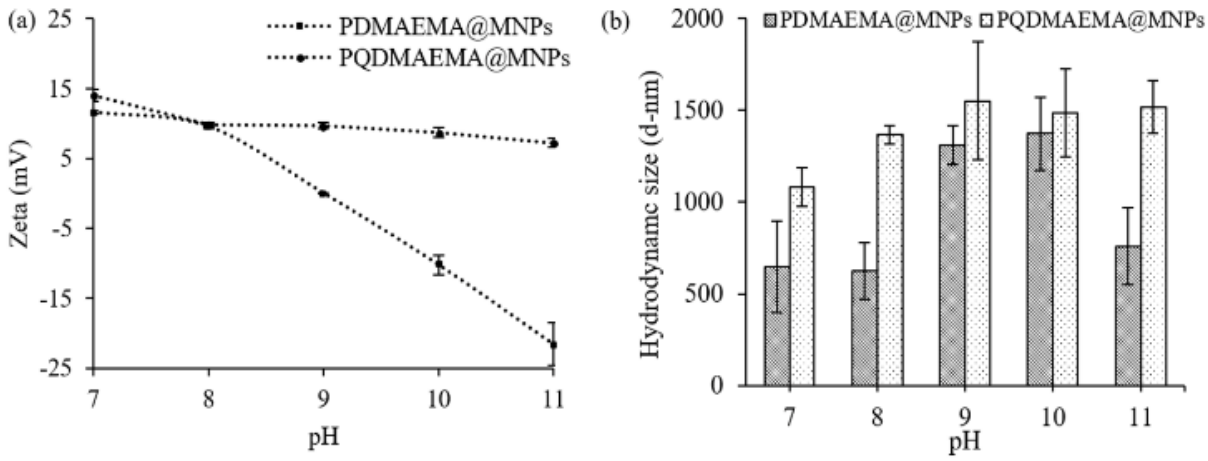

Figure 4. (a) Zeta potential and (b) hydrodynamic size (D_h) of PDMAEMA @MNPs and PQDMAEMA@MNPs.

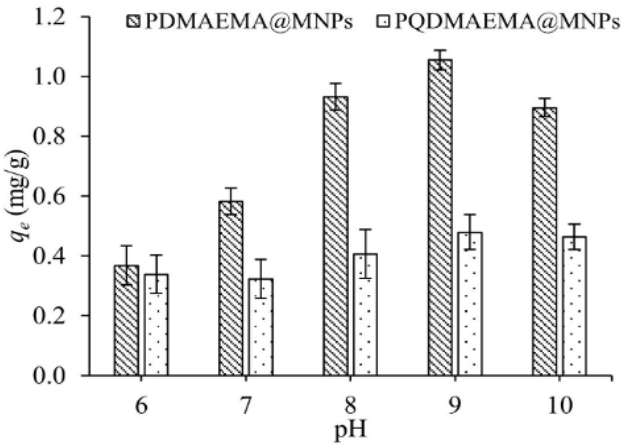

Figure 5. The BPA adsorption capacity (q_e) on PDMAEMA@MNPs and PQDMAEMA@MNPs in phosphate buffer solutions (pH 6 to pH 10).

3.3 The desorption of BPA from PDMAEMA@MNPs

Previous works have reported that methanol can be effectively used to desorb BPA from adsorbents by weakening the interaction between BPA and the adsorbent surface [5,46-48]. Methanol was thus used as a washing solution for desorption of BPA from the MNPs in this work. The signals of BPA in the washing solutions were quantitatively analyzed *via* HPLC-DAD and the washing process was repeated until the signals of BPA in the washing solutions were not observed. It was found that 99.8% desorption efficiency of BPA was observed after the first washing and it was completely removed from the particle surface after three-time washings. The desorption efficiency (%) of BPA and other desorption results are shown in the supporting information (Figure S3 and S4). These results were in good agreement with those obtained from EDX technique, investigating the ratio of C/Fe of the nano-adsorbents before and after the BPA adsorption. It was hypothesized that the increase in C/Fe ratio implied the increase of BPA in the nano-adsorbent. It was found that the C/Fe ratio increased from 0.35 to 0.77 after the BPA adsorption step (Figure 6 and Table S1). After washing with methanol, the C/Fe ratio significantly dropped to 0.31 and this value was close to the initial C/Fe ratio (0.35). These EDX results signified the effective removal of BPA from the MNPs by simply washing with methanol. From the morphological study *via* SEM, PDMAEMA@MNPs exhibited average diameter of *ca*.10 nm to 20 nm, and they showed some degree of particle aggregation after BPA adsorption (Figure S5). After washing with methanol to remove BPA, the morphology and size of the particles were somewhat similar to those before BPA adsorption.

3.4 The study in the adsorption isotherms

The concentration dependence of BPA adsorption on PDMAEMA @MNPs was investigated. The BPA adsorption experiment was carried out in the concentration range from 10 to 200 ppm with 2 mg of MNPs used. The amount of BPA adsorbed increased with increasing BPA concentration up to 50 ppm where the percentage of BPA adsorbed on the nanoparticles is 79% (10 mg·g^{-1} MNPs) (Figure 7(b)). An example of the calculation of the percent BPA adsorbed on the MNPs is shown in the supporting information. The percentage of adsorbed BPA initially increased rapidly due to the availability of large numbers of active sites on the particle surface, and slightly decreased when high BPA concentrations were used [12]. The adsorption kinetics of BPA on the MNPs was studied with 50-ppm BPA concentration during a 30-min time interval. The BPA adsorption on the MNPs reached equilibrium within 5 min and the observed adsorption capacity (q_e) is 9.88 mg·g^{-1} (Figure 7(b)). These results indicated that PDMAEMA@MNPs had high BPA adsorption capacity as compared to those previously reported (Table 2). The rapid adsorption of BPA was explained in terms of facile availability of the adsorption sites on the particle surface. As the adsorption time was extended, the adsorption capacity decreased due to the decrease of available adsorption sites [49].

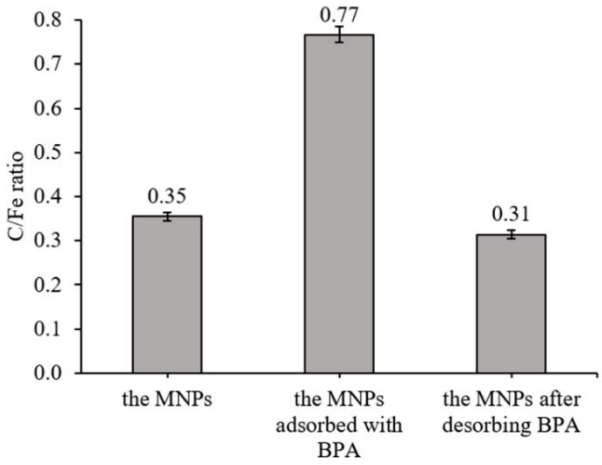

Figure 6. The ratio of C/Fe of PDMAEMA@MNPs obtained from SEM-EDX technique.

Table 2. The comparison in the adsorption capability of BPA on the adsorbents of this work (PDMAEMA@MNPs) with those from other reports.

Adsorbents	**Techniques**	**Adsorption Capacity (mg·g^{-1})**	**Reference**
Magnetite nanoparticles coated with PDMAEMA	HPLC-DAD	9.88	This work
Magnetite nanoparticles	UV/Visible	4.511	[12]
Magnetic hydrophilic molecularly imprinted material (MIM)	HPLC-DAD	8.97	[2]
Surface modification of waste biomass: banana bunch and coconut bunch	UV/Visible	4.53, 4.66	[11]
Surfactant-modified natural zeolite:	UV/Visible	6.8	[50]
Activated carbon of banana fronds (*Musa acuminata*)	UV/Visible	1.3	[51]

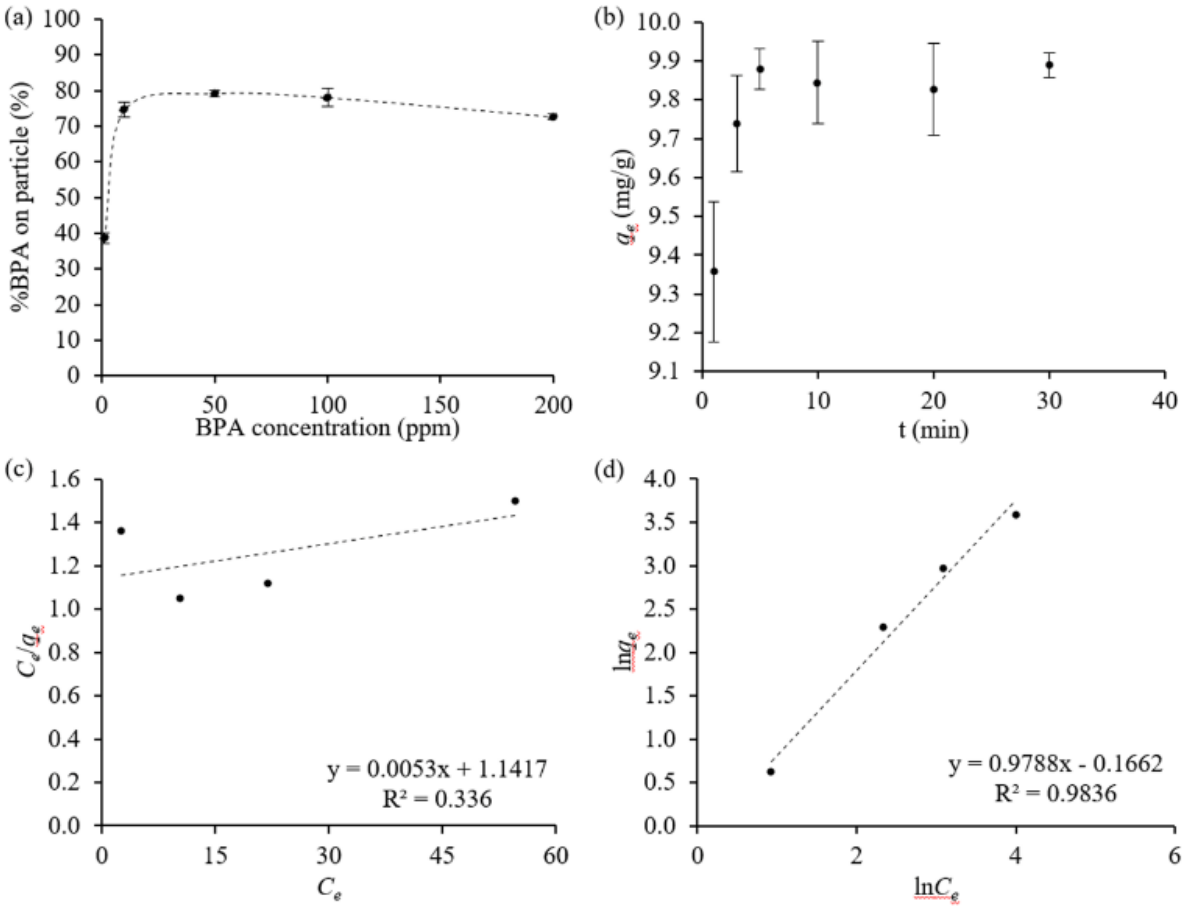

Figure 7. (a) The percentage of BPA adsorption on PDMAEMA@MNPs, (b) effect of time on BPA adsorption on PDMAEMA@MNPs, (c) the Langmuir isotherm plot, (d) the Freundlich isotherm plot of BPA adsorption on PDMAEMA@MNPs.

The isotherm plots for the BPA adsorption process are shown in Figure 7(c) and 7(d). The BPA adsorption on the MNPs was correlated with the Langmuir and Freundlich adsorption models and the isotherm parameters, which were calculated from the intercepts and the slopes of the plots, are shown in Table 3. The Freundlich isotherm model assumes a multilayered adsorption through the interaction between the surface of the adsorbent and the adsorbate molecules [52]. On the other hand, the Langmuir isotherm model assumes a monolayer adsorption without any interaction with the adjacent sites on the solid support. Based on the regression coefficients (R^2 value), the Freundlich model (R^2=0.9836) provided a better fit than the Langmuir model (R^2=0.336), suggesting that a multilayer coverage of the nano-adsorbent surface provided a better description of the process. An example of the adsorption isotherm calculation is shown in the supporting information.

3.5 Investigation of the adsorption kinetics

The linear pseudo-first-order plot and the pseudo-second-order plot are shown in Figure 8(a) and 8(b). It was found that the adsorption kinetic data fit the linear pseudo-second order model with R^2=1.000 with the adsorption capacity (q_e) value of 9.891 mg·g^{-1}. The kinetic parameters obtained from these two plots are shown in Table 4 and an example of the calculation is shown in the supporting information. This finding agrees well with the adsorption capacity (q_e) obtained from the experimental data shown in Figure 8(a). These results indicate that the linear pseudo- second- order kinetic model gives a good correlation for BPA adsorption process on the PDMAEMA@MNPs and corresponds well with a previous report [53].

Table 3. Isotherm parameters of BPA adsorption on PDMAEMA@MNPs.

Isotherm	Parameters	Values
Langmuir	q_m (mg·g^{-1})	188.679
	K_L (L·mg^{-1})	0.006
	R^2	0.336
Freundlich	K_f (mg·g^{-1})	0.871
	n	1.022
	R^2	0.984

Table 4. Kinetic parameters.

Kinetic model	Parameters	Values
Pseudo-first-order kinetics	q_e (mg·g^{-1})	0.046
	k_1 (min^{-1})	0.062
	R^2	0.124
Pseudo-second-order kinetics	q_e (mg·g^{-1})	9.891
	k_2 (g·mg^{-1}·min^{-1})	0.000
	R^2	1.000

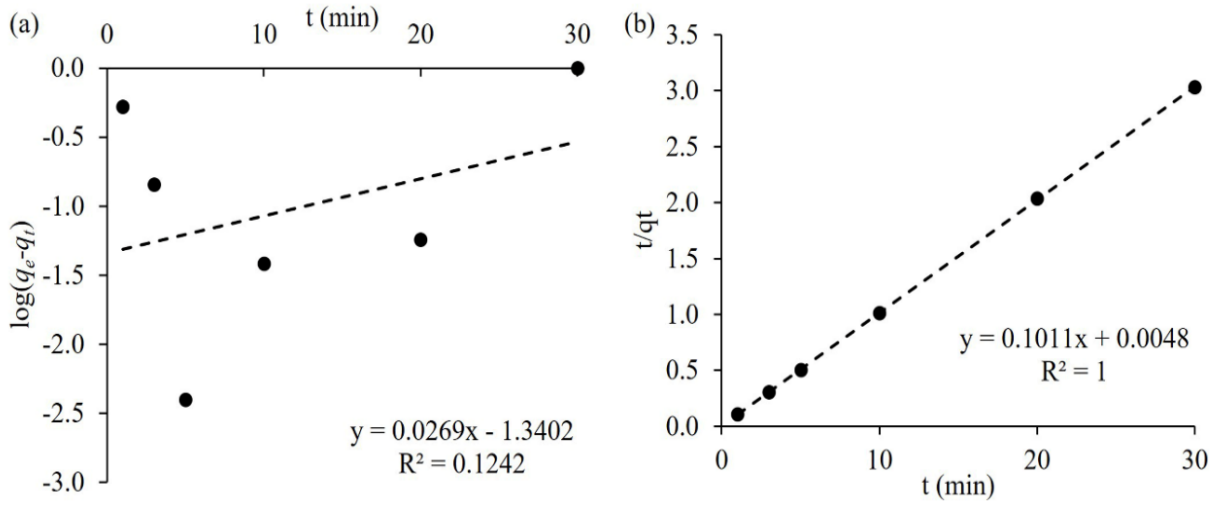

Figure 8. (a) The pseudo-first-order plot, (b) the pseudo-second-order plot.

In addition, the pseudo first order and the pseudo second-order kinetics using the non-linear regression method were also calculated and the parameters were provided in the supporting information (Figure S6 and Table S2). The OriginPro software [54,55] was used for determining the pseudo-first-order and pseudo-second-order kinetic parameters. As discussed in more detail in the supporting information, the values of the various parameters calculated from the linear method when compared to the non-linear method suggested the use of the linear method for the prediction of the adsorption kinetics in the current work.

3.6 Investigation of the intraparticle diffusion model and the adsorption mechanism

The intraparticle diffusion model based on Equation (9) [19] was used to study the adsorption mechanism.

$$q_t = k_i t^{0.5} + C \quad (9)$$

where q_t is the amount of BPA adsorbed at a given time (mg·g^{-1}), k_i is intraparticle diffusion rate constant (mg·g·min$^{0.5}$), $t^{0.5}$ is the square root of time (min$^{0.5}$), and C is intercept. The plot of q_t versus $t^{0.5}$ for PDMAEMA@MNPs revealed that the plot was multilinearity, implying that the adsorption process had two or more phases [56,57] (Figure 9). It shows an initial stage with a high slope value, representing the BPA affinity toward the MNP surface facilitated by hydrogen bonding interactions between BPA and PDMAEMA on the MNPs. This was a fast process and completed within 5 min. The second stage showed the effect of pore diffusion or intraparticle diffusion, which was the process where the BPA molecules transferred from the MNP surface into the inner polymer layer by physical adsorption. This stage took 5 min to 30 min and was slower than those in the first stage. It was hypothesized that the hydrogen bonding existing on the MNPs somewhat reduced the diffusion process and essentially enhanced the adsorption [8,15]. In the last stage, the adsorption reached the equilibrium, signifying the saturation of the adsorption sites and this took *ca.*30 min after the initiation. The k_i values and other parameters are listed in Table 5.

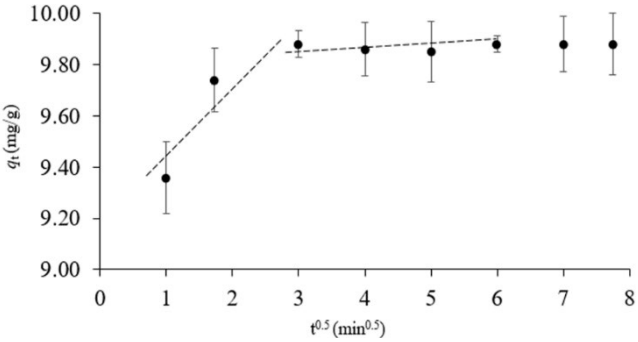

Figure 9. The intraparticle diffusion model for BPA adsorption on PDMAEMA@MNPs

Table 5. The intraparticle diffusion model parameters for BPA adsorption on PDMAEMA@MNPs.

Stage	k_i (mg·g^{-1}·min$^{0.5}$)	C (mg·g^{-1})	R^2
First	0.244	9.19	0.9374
Second	0.007	9.83	0.6296

The proposed adsorption mechanism of BPA on PDMAEMA @MNP surface are shown in the supporting information (Figure S7). The main adsorption interaction between BPA and the particles was the hydrogen bonding between the hydroxyl groups of BPA and amino/ ester groups of PDMAEMA on the MNPs [1,8,15].

3.7 Investigation of the adsorption thermodynamics

The effect of the temperature change on their adsorption capacity was investigated in the temperature range from 30°C to 70°C (303 K to 343 K) using 50-ppm BPA and 2-mg of the MNPs (Figure 8). It was found that the BPA adsorption capacity (q_e) decreased when increasing the temperature, and this was attributed to the physisorption between BPA and the MNP surface (Figure 10). The thermodynamic parameters, including standard enthalpy change (ΔH°), standard entropy change (ΔS°), and standard Gibbs free energy change (ΔG°), giving the information about internal energy changes during the BPA adsorption

on the MNPs, are shown in Table 6 and the examples of the calculations are shown in the supporting information. The negative values of ΔG° signify a spontaneous nature of the BPA adsorption process. In addition, the negative value of ΔH° (-2585.571 J·mol^{-1}) and the positive value of ΔS° (1.309 J·mol^{-1}·K) suggest an exothermic adsorption process of BPA on the MNPs. These results indicate the decrease in BPA adsorption capacity when increasing temperature.

3.8 Study in the regeneration and stability of the adsorbents

The adsorbents with good regeneration ability can be advantageous for the reuse purpose. Many researches have focused on the regeneration of the adsorbent while maintaining its good stability on order to decrease the cost of the process by reusing it [5,10,18,56]. In this work, PDMAEMA@MNPs were reused for BPA adsorption for four cycles and tested with XRD technique to investigate their stability. Methanol was used as a washing solvent to desorb BPA from the particles in each cycle due to its effective washing ability as discussed above.

The XRD patterns of the regenerated MNPs after the reuse for four cycles retained their characteristic signals of magnetite crystal structure as compared to those before BPA adsorption and the standard Fe_3O_4 powder diffraction data (JCPDS 00-019-0629) [58] as shown in Figure 11. These results indicated the good stability of the MNPs after four cycles of their reuse.

Table 6. Thermodynamic parameters.

Temperature (K)	ΔH° (J·mol^{-1})	ΔS° (J·mol^{-1}·K)	ΔG° (J·mol^{-1})
303	-2585.571	1.309	-2982.336
313			-2995.430
323			-3008.525
343			-3034.714

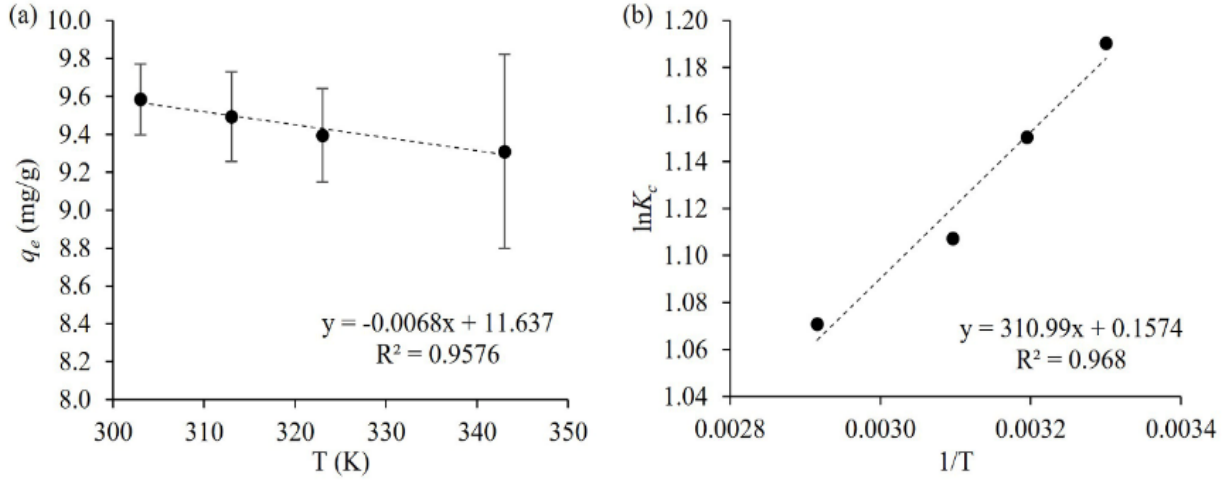

Figure 10. (a) Effect of the temperature change on BPA adsorption on PDMAEMA@MNPs, and (b) the thermodynamic plot.

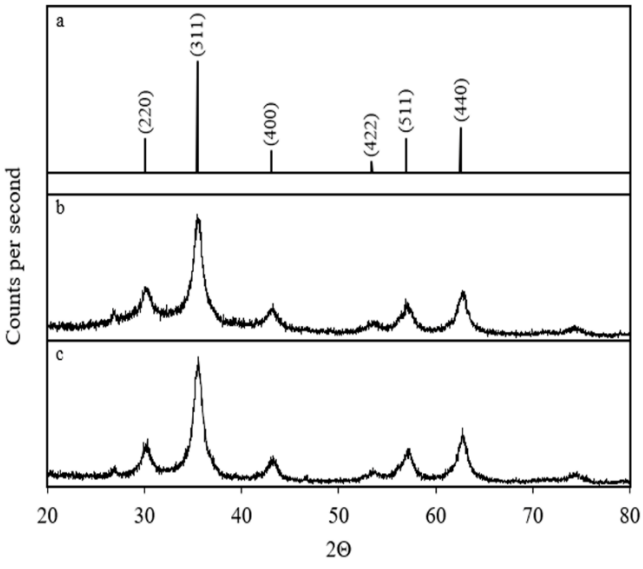

Figure 11. XRD patterns of (a) the standard Fe_3O_4 powder diffraction data (JCPDS 00-019-0629), (b) the regenerated MNPs after the reuse for four cycles and (c) the MNPs before the BPA adsorption

4. Conclusions

Nano-adsorbents with different surface charges (PDMAEMA @MNPs and PQDMAEMA@MNPs) were successfully synthesized and used for BPA adsorption. They show good magnetic responsiveness, good water dispersibility, and high adsorption capacity for BPA. PDMAEMA@MNPs exhibited a higher adsorption capacity than their quarternized form due to their high surface area, pore volume and pore size. The BPA adsorption of PDMAEMA@MNPs reached the equilibrium within 5 min with the maximum adsorption capacity (qe) of 9.88 mg/g, and it followed the Freundlich model, suggesting a multilayer coverage of the adsorbent surface. The adsorption kinetics corresponded well to a pseudo-second order process with a regression coefficient value of 1.00. BPA initially interacted with PDMAEMA on the MNPs mainly by hydrogen bonding, followed by the diffusion from the surface into the inner polymer layer by physical adsorption. The observed thermodynamic data shows that the adsorption process was exothermic and spontaneous in nature as indicated by the ΔH° and ΔG° values. The investigated nano-adsorbents might potentially be used for the BPA adsorption and for the detection of BPA contamination in samples of interest.

Acknowledgements

BR acknowledges the Faculty of Science, Naresuan University (R2564E025) for financial support. JT thanks the Science Achievement Scholarship of Thailand (SAST) for the scholarship.

References

[1] L. Cui, J. Wei, X. Du, and X. Zhou, "Preparation and evaluation of self-assembled porous microspheres–fibers for removal of bisphenol A from aqueous solution," *Industrial & engineering chemistry research,* vol. 55, no. 6, pp. 1566-1574, 2016.

[2] H. Xiong, L. Guo, X. Mao, T. Tan, H. Wan, and Y. Wan, "A magnetic hydrophilic molecularly imprinted material with multiple stimuli-response properties for efficient recognition of bisphenol A in beverages," *Food Chemistry,* vol. 331, p. 127311, 2020.

[3] J. H. Kang, D. Aasi, and Y. Katayama, "Bisphenol A in the aquatic environment and its endocrine-disruptive effects on aquatic organisms," *Critical reviews in toxicology,* vol. 37, no. 7, pp. 607-625, 2007.

[4] M. Martín-Lara, M. Calero, A. Ronda, I. Iáñez-Rodríguez, and C. Escudero, "Adsorptive behavior of an activated carbon for bisphenol A removal in single and binary (bisphenol A—heavy metal) solutions," *Water,* vol. 12, no. 8, p. 2150, 2020.

[5] K. Ragavan, and N. K. Rastogi, "β-Cyclodextrin capped graphene-magnetite nanocomposite for selective adsorption of Bisphenol-A," *Carbohydrate polymers,* vol. 168, pp. 129-137, 2017.

[6] D. Balarak, F. K. Mostafapour, S. M. Lee, and C. Jeon, "Adsorption of bisphenol a using dried rice husk: equilibrium, kinetic and thermodynamic studies," *Applied Chemistry for Engineering,* vol. 30, no. 3, pp. 316-323, 2019.

[7] S. Rovani, J. J. Santos, S. N. Guilhen, P. Corio, and D. A. Fungaro, "Fast, efficient and clean adsorption of bisphenol-A using renewable mesoporous silica nanoparticles from sugarcane waste ash," *RSC Advances,* vol. 10, no. 46, pp. 27706-27712, 2020.

[8] X. Zhou, J. Wei, K. Liu, N. Liu, and B. Zhou, "Adsorption of bisphenol A based on synergy between hydrogen bonding and hydrophobic interaction," *Langmuir,* vol. 30, no. 46, pp. 13861-13868, 2014.

[9] M. A. Zazouli, F. Veisi, and A. Veisi, "Modeling of Bisphenol A (BPA) Removal from Aqueous Solutions by Adsorption Using Response Surface Methodology (RSM)," *International Journal of Chemical and Molecular Engineering,* vol. 10, no. 2, pp. 228-233, 2016.

[10] Q. Li, F. Pan, W. Li, D. Li, H. Xu, D. Xia, and A. Li, "Enhanced adsorption of bisphenol A from aqueous solution with 2-vinylpyridine functionalized magnetic nanoparticles," *Polymers,* vol. 10, no. 10, p. 1136, 2018.

[11] H. Abdullah, M. Nuid, N. A. A. Salim, N. A. Zainuddin, and N. Ahmad, "Bisphenol A Removal by Adsorption Using Waste Biomass: Isotherm and Kinetic Studies," *Biointerface Research in Applied Chemistry,* vol. 11, no. 1, pp. 8467-8481, 2021.

[12] B. Orimolade, F. Adekola, and G. Adebayo, "Adsorptive removal of bisphenol A using synthesized magnetite nanoparticles," *Applied water science,* vol. 8, no. 1, pp. 1-8, 2018.

[13] M. B. Ahmed, J. L. Zhou, H. H. Ngo, W. Guo, N. S. Thomaidis, and J. Xu, "Progress in the biological and chemical treatment technologies for emerging contaminant removal from wastewater: a critical review," *Journal of hazardous materials,* vol. 323, pp. 274-298, 2017.

[14] D. Bing-zhi, C. Hua-qiang, W. Lin, X. Sheng-ji, and G. Nai-yun, "The removal of bisphenol A by hollow fiber microfiltration membrane," *Desalination,* vol. 250, no. 2, pp. 693-697, 2010.

[15] J. Wang, and M. Zhang, "Adsorption characteristics and mechanism of bisphenol A by magnetic biochar," *International journal of environmental research and public health,* vol. 17, no. 3, p. 1075, 2020.

[16] M. El-Bindary, M. El-Desouky, and A. El-Bindary, "Adsorption of industrial dye from aqueous solutions onto thermally treated green adsorbent: A complete batch system evaluation," *Journal of Molecular Liquids,* vol. 346, p. 117082, 2022.

[17] K. Elwakeel, A. El-Bindary, and E. Kouta, "Retention of copper, cadmium and lead from water by Na-Y-Zeolite confined in methyl methacrylate shell," *Journal of environmental chemical engineering,* vol. 5, no. 4, pp. 3698-3710, 2017.

[18] H. A. Kiwaan, T. M. Atwee, E. A. Azab, and A. A. El-Bindary, "Efficient photocatalytic degradation of Acid Red 57 using synthesized ZnO nanowires," *Journal of the Chinese Chemical Society,* vol. 66, no. 1, pp. 89-98, 2019.

[19] N. Hassan, A. Shahat, A. El-Didamony, M. El-Desouky, and A. El-Bindary, "Synthesis and characterization of ZnO nanoparticles via zeolitic imidazolate framework-8 and its application for removal of dyes," *Journal of molecular structure,* vol. 1210, p. 128029, 2020.

[20] Y. Su, C. Shao, X. Huang, J. Qi, R. Ge, H. Guan, and Z. Lin, "Extraction and detection of bisphenol A in human serum and urine by aptamer-functionalized magnetic nanoparticles," *Analytical and bioanalytical chemistry,* vol. 410, no. 7, pp. 1885-1891, 2018.

[21] P. Theamdee, B. Rutnakornpituk, U. Wichai, and M. Rutnakornpituk, "Recyclable magnetic nanoparticle grafted with pH-responsive polymer for adsorption with DNA," *Journal of nanoparticle research,* vol. 16, no. 7, pp. 1-12, 2014.

[22] B. Rutnakornpituk, T. Theppaleak, M. Rutnakornpituk, and T. Vilaivan, "Recyclable magnetite nanoparticle coated with cationic polymers for adsorption of DNA," *Journal of Biomaterials science, Polymer edition,* vol. 27, no. 11, pp. 1200-1210, 2016.

[23] N. Deepuppha, S. Khadsai, B. Rutnakornpituk, F. Kielar, and M. Rutnakornpituk, "Reusable pectin-coated magnetic nanosorbent functionalized with an aptamer for highly selective Hg2+ detection," *Polymers for Advanced Technologies,* vol. 32, no. 5, pp. 2207-2217, 2021.

[24] X. Wu, Y. Li, X. Zhu, C. He, Q. Wang, and S. Liu, "Dummy molecularly imprinted magnetic nanoparticles for dispersive solid-phase extraction and determination of bisphenol A in water samples and orange juice," *Talanta,* vol. 162, pp. 57-64, 2017.

[25] J. Connolly, T. St Pierre, M. Rutnakornpituk, and J. Riffle, "Silica coating of cobalt nanoparticles increases their magnetic and chemical stability for biomedical applications," *European Cells and Materials,* vol. 3, no. 2, pp. 106-109, 2002.

[26] M. Rutnakornpituk, V. Baranauskas, J. Riffle, J. Connolly, T. St Pierre, and J. Dailey, "Polysiloxane fluid dispersions of Cobalt nanoparticles in silica spheres for use in opthalmic applications," *European Cells and Materials,* vol. 3, no. 2, pp. 102-105, 2002.

[27] S. Khadsai, B. Rutnakornpituk, T. Vilaivan, M. Nakkuntod, and M. Rutnakornpituk, "Anionic magnetite nanoparticle conjugated with pyrrolidinyl peptide nucleic acid for DNA base discrimination," *Journal of Nanoparticle Research,* vol. 18, no. 9, pp. 1-15, 2016.

[28] B. Rutnakornpituk, U. Wichai, T. Vilaivan, and M. Rutnakornpituk, "Surface-initiated atom transfer radical polymerization of poly (4-vinylpyridine) from magnetite nanoparticle," *Journal of Nanoparticle Research,* vol. 13, no. 12, pp. 6847-6857, 2011.

[29] S. Meerod, B. Rutnakornpituk, U. Wichai, and M. Rutnakornpituk, "Hydrophilic magnetic nanoclusters with thermo-responsive properties and their drug controlled release," *Journal of Magnetism and Magnetic Materials,* vol. 392, pp. 83-90, 2015.

[30] T. Theppaleak, G. Tumcharern, U. Wichai, and M. Rutnakornpituk, "Synthesis of water dispersible magnetite nanoparticles in the presence of hydrophilic polymers," *Polymer bulletin,* vol. 63, no. 1, pp. 79-90, 2009.

[31] N. Deepuppha, A. Thongsaw, B. Rutnakornpituk, W. C. Chaiyasith, and M. Rutnakornpituk, "Alginate-based magnetic nanosorbent immobilized with aptamer for selective and high adsorption of Hg 2+ in water samples," *Environmental Science and Pollution Research,* vol. 27, no. 11, pp. 12030-12038, 2020.

[32] S. Meerod, N. Deepuppha, B. Rutnakornpituk, and M. Rutnakornpituk, "Reusable magnetic nanocluster coated with poly (acrylic acid) and its adsorption with an antibody and an antigen," *Journal of Applied Polymer Science,* vol. 135, no. 16, p. 46160, 2018.

[33] S. Khadsai, N. Seeja, N. Deepuppha, M. Rutnakornpituk, T. Vilaivan, M. Nakkuntod, and B. Rutnakornpituk, "Poly (acrylic acid)-grafted magnetite nanoparticle conjugated with pyrrolidinyl peptide nucleic acid for specific adsorption with real DNA," *Colloids and Surfaces B: Biointerfaces,* vol. 165, pp. 243-251, 2018.

[34] P. Theamdee, R. Traiphol, B. Rutnakornpituk, U. Wichai, and M. Rutnakornpituk, "Surface modification of magnetite nanoparticle with azobenzene-containing water dispersible polymer," *Journal of Nanoparticle Research,* vol. 13, no. 10, pp. 4463-4477, 2011.

[35] M. A. De Jesús-Téllez, D. M. Sánchez-Cerrillo, P. Quintana-Owen, U. S. Schubert, D. Contreras-López, and C. Guerrero-Sánchez, "Kinetic investigations of quaternization reactions of poly [2-(dimethylamino) ethyl methacrylate] with diverse alkyl halides," *Macromolecular Chemistry and Physics,* vol. 221, no. 9, p. 1900543, 2020.

[36] Z. Dong, H. Wei, J. Mao, D. Wang, M. Yang, S. Bo, and X. Ji, "Synthesis and responsive behavior of poly (N, N-dimethyl-aminoethyl methacrylate) brushes grafted on silica nanoparticles and their quaternized derivatives," *Polymer,* vol. 53, no. 10, pp. 2074-2084, 2012.

[37] A. B. Shatan, V. Patsula, A Dydowiczova, K. Gunar, N. Velychkivska, J. Hromadkova, E. Petrovsky, and D. Horak, "Cationic Polymer-Coated Magnetic Nanoparticles with Antibacterial Properties: Synthesis and In Vitro Characterization," *Antibiotics,* vol. 10, no. 9, p. 1077, 2021.

[38] T. Theppaleak, B. Rutnakornpituk, U. Wichai, T. Vilaivan, and M. Rutnakornpituk, "Magnetite nanoparticle with positively charged surface for immobilization of peptide nucleic acid and deoxyribonucleic acid," *Journal of biomedical nanotechnology,* vol. 9, no. 9, pp. 1509-1520, 2013.

[39] F. Adekola, D. Hodonou, and H. Adegoke, "Thermodynamic and kinetic studies of biosorption of iron and manganese from aqueous medium using rice husk ash," *Applied Water Science,* vol. 6, no. 4, pp. 319-330, 2016.

[40] C. A. Dinçer, N. Yıldız, N. Aydoğan, and A. Çalımlı, "A comparative study of Fe3O4 nanoparticles modified with different silane compounds," *Applied surface science,* vol. 318, pp. 297-304, 2014.

[41] P. Jiang, G. Li, L. Lv, H. Ji, Z. Li, S. Chen, and S. Chu, "Effect of DMAEMA content and polymerization mode on morphologies and properties of pH and temperature double-sensitive cellulose-based hydrogels," *Journal of Macromolecular Science, Part A,* vol. 57, no. 3, pp. 207-216, 2020.

[42] A. Hernández-Martínez and E. Bucio, "Novel pH-and temperature-sensitive behavior of binary graft DMAEMA/PEGMEMA onto LDPE membranes," *Designed monomers and polymers,* vol. 12, no. 6, pp. 543-552, 2009.

[43] G. Estrada-Villegas, and E. Bucio, "Temperature-and pH-responsive behavior of a novel copolymer of (PP-g-DMAEMA)-g-AAc," *Journal of Radioanalytical and Nuclear Chemistry,* vol. 292, no. 1, pp. 1-6, 2012.

[44] L. Xu, J. Zhang, J. Ding, T. Liu, G. Shi, X. Li, W. Dang, Y. Cheng, and R. Guo, "Pore structure and fractal characteristics of different shale lithofacies in the dalong formation in the western area of the lower yangtze platform," *Minerals,* vol. 10, no. 1, p. 72, 2020.

[45] F. Wang, Q. Zeng, W. Su, M. Zhang, L. Hou, and Z. L. Wang, "Adsorption of bisphenol A on peanut shell biochars: The effects of surfactants," *Journal of Chemistry,* vol. 2019, 2019.

[46] Y. Zhang, Y. Cheng, N. Chen, Y. Zhou, B. Li, W. Gu, X. Shi, and Y. Xian, "Recyclable removal of bisphenol A from aqueous solution by reduced graphene oxide–magnetic nanoparticles: adsorption and desorption," *Journal of colloid and interface science,* vol. 421, pp. 85-92, 2014.

[47] Y. Li, P. Lu, J. Cheng, X. Zhu, W. Guo, L. Liu, Q. Wang, C. He, and S. Liu, "Novel microporous β-cyclodextrin polymer as sorbent for solid-phase extraction of bisphenols in water samples and orange juice," *Talanta,* vol. 187, pp. 207-215, 2018.

[48] C. Cáceres, C. Bravo, B. Rivas, E. Moczko, P. Saez, Y. Garcia, and E. Pereira, "Molecularly imprinted polymers for the selective extraction of bisphenol a and progesterone from aqueous media," *Polymers,* vol. 10, no. 6, p. 679, 2018.

[49] G. Zeng, C. Zhang, G. Huang, J. Yu, Q. Wang, J. Li, B. Xi, and H. Liu, "Adsorption behavior of bisphenol A on sediments

in Xiangjiang River, Central-south China," *Chemosphere,* vol. 65, no. 9, pp. 1490-1499, 2006.

[50] N. Genç, Ö. Kılıçoğlu, and A. O. Narci, "Removal of Bisphenol A aqueous solution using surfactant-modified natural zeolite: Taguchi's experimental design, adsorption kinetic, equilibrium and thermodynamic study," *Environmental Technology,* vol. 38, no. 4, pp. 424-432, 2017.

[51] N. Rahmat, T. Hadibarata, A. Yuniarto, M. Elshikh, and A. Syafiuddin, "Isotherm and kinetics studies for the adsorption of bisphenol A from aqueous solution by activated carbon of Musa acuminata," in *IOP Conference Series: Materials Science and Engineering*, 2019, vol. 495, no. 1: IOP Publishing, p. 012059.

[52] K. Y. Foo, and B. H. Hameed, "Insights into the modeling of adsorption isotherm systems," *Chemical engineering journal,* vol. 156, no. 1, pp. 2-10, 2010.

[53] M. H. Dehghani, M. Ghadermazi, A. Bhatnagar, P. Sadighara, G. Jahed-Knaniki, B. Heibati, and G. McKay, "Adsorptive removal of endocrine disrupting bisphenol A from aqueous solution using chitosan," *Journal of Environmental Chemical Engineering,* vol. 4, no. 3, pp. 2647-2655, 2016.

[54] K. V. Kumar, "Linear and non-linear regression analysis for the sorption kinetics of methylene blue onto activated carbon," *Journal of hazardous materials,* vol. 137, no. 3, pp. 1538-1544, 2006.

[55] S. Chowdhury, and P. Saha, "Adsorption kinetic modeling of safranin onto rice husk biomatrix using pseudo-first-and pseudo-second-order kinetic models: Comparison of linear and non-linear methods," *CLEAN–Soil, Air, Water,* vol. 39, no. 3, pp. 274-282, 2011.

[56] G. A. AlHazmi, K. S. AbouMelha, M. G. El-Desouky, and A. A. El-Bindary, "Effective adsorption of doxorubicin hydrochloride on zirconium metal-organic framework: Equilibrium, kinetic and thermodynamic studies," *Journal of Molecular Structure,* vol. 1258, p. 132679, 2022.

[57] A. E. Ofomaja, E. B. Naidoo, and A. Pholosi, "Intraparticle diffusion of Cr (VI) through biomass and magnetite coated biomass: A comparative kinetic and diffusion study," *South African Journal of Chemical Engineering,* vol. 32, no. 1, pp. 39-55, 2020.

[58] V. A. R. Villegas, J. I. D. L. Ramírez, E. H. Guevara, S. P. Sicairos, L. A. H. Ayala, and B. L. Sanchez, "Synthesis and characterization of magnetite nanoparticles for photocatalysis of nitrobenzene," *Journal of Saudi Chemical Society,* vol. 24, no. 2, pp. 223-235, 2020.